Ballistic Lunar Transfers to Near Rectilinear Halo Orbit: Operational Considerations

Nathan L. Parrish[1], Ethan W. Kayser[2], Matthew J. Bolliger[3],
Michael R. Thompson[4], Jeffrey S. Parker[5], Bradley W. Cheetham[6]
Advanced Space LLC, 2100 Central Ave, Boulder, CO 80301

Diane C. Davis[7]
ai solutions, 2224 Bay Area Blvd #415, Houston, TX 77058

Daniel J. Sweeney[8]
NASA Johnson Space Center, Houston TX 77048

This paper presents a study of ballistic lunar transfer (BLT) trajectories from Earth launch to insertion into a near rectilinear halo orbit (NRHO). BLTs have favorable properties for uncrewed launches to orbits in the vicinity of the Moon, such as dramatically reduced spacecraft ΔV requirements. Results are described from a detailed set of related mission design and navigation studies: maneuver placement, tracking cadence, and statistical ΔV requirements for various navigation state errors. Monte Carlo analyses are presented which simulate BLT navigation with various DSN tracking schedules. These analyses are presented to inform future missions to NRHOs.

I. Introduction

A. Motivation

The Gateway is proposed as the next human outpost in space; a proving ground near the Moon for deep space technologies and a staging location for missions beyond Earth orbit and to the lunar surface. As the Gateway is constructed over time, both crewed and uncrewed payloads will frequently travel to the spacecraft. Examples include elements of the Gateway itself as the spacecraft grows in size, logistics modules carrying supplies, Human Lander System (HLS) elements to support a crewed lunar landing, and the Orion crew vehicle. Minimizing the cost of transfer from Earth to the Gateway enables successful construction, operations, and exploration.

The Gateway is planned to orbit the Moon in a Near Rectilinear Halo Orbit (NRHO), a nearly stable member of the L_2 Halo family of orbits. The NRHO proposed for the primary Gateway orbit is characterized by a perilune radius of approximately 3,500 km and an apolune radius of about 71,000 km over the lunar south pole. With an orbital period of about 6.5 days, the southern L_2 NRHO exhibits a 9:2 resonance with the lunar synodic period. A low-energy orbit, the NRHO sits at the top of the lunar gravity well, and thus, insertion into orbit requires much less ΔV than for a low lunar orbit. Nevertheless, fast transfers from the Earth to NRHO require significant ΔV.[1] For uncrewed spacecraft without strict constraints on flight time, significant propellant savings can be achieved by allowing longer times of flight and employing the effects of solar gravity to naturally raise the orbit to the Moon. Such transfers are known as Ballistic Lunar Transfers (BLTs). Many previous investigations have explored the use of BLTs for transfer to various multibody orbits, both unstable[2] and stable.[3] BLTs have successfully been employed for transfer of several spacecraft to lunar orbits, including the Hiten [4] and GRAIL [5] missions. A previous study[6] surveyed the use of BLTs for transfer

[1] Optimization Lead, Advanced Space, LLC, 2100 Central Ave STE 102, Boulder, CO 80301. AIAA member.
[2] Aerospace Engineer, Advanced Space, LLC, 2100 Central Ave STE 102, Boulder, CO 80301. AIAA member.
[3] Aerospace Engineer, Advanced Space, LLC, 2100 Central Ave STE 102, Boulder, CO 80301. AIAA member.
[4] Aerospace Engineer, Advanced Space, LLC, 2100 Central Ave STE 102, Boulder, CO 80301. AIAA member.
[5] Chief Technical Officer, Advanced Space, LLC, 2100 Central Ave STE 102, Boulder, CO 80301. AIAA member.
[6] Chief Executive Officer, Advanced Space, LLC, 2100 Central Ave STE 102, Boulder, CO 80301. AIAA member.
[7] Principal Systems Engineer, ai solutions, 2224 Bay Area Blvd #415, Houston, TX 77058. AIAA member.
[8] Gateway Integrated Spacecraft Performance Lead, NASA Johnson Space Center, Houston, TX 77058. AIAA member.

to the Gateway NRHO, finding that BLTs increase the cargo mass delivered to an NRHO by 8-12% compared to direct transfers.

The current investigation explores operational considerations for BLTs to the NRHO. First, launch opportunities are investigated that allow near-simultaneous arrival of multiple spacecraft launched in subsequent months. Then, the sensitivities of the BLT trajectories to launch and maneuver execution errors are assessed, and a schedule of Trajectory Correction Maneuvers (TCMs) is proposed. Finally, orbit determination and tracking schedules are considered for BLTs to the NRHO.

B. Background

Ballistic Lunar Transfers (BLTs) exist for a variety of 3-body orbits.[2] In these transfer orbits, the Sun's gravity is used to raise perigee and adjust inclination. In order for the Sun's gravity to have a significant effect on the trajectory, the apogee must be approximately 1-2 million kilometers. A true "ballistic" transfer has no deterministic maneuvers required after launch, asymptotically approaching the target 3-body orbit along its unstable manifold or, in some cases, along a trajectory that harnesses perturbations without an unstable manifold [3]. In the literature, studies of BLTs in the Sun-Earth circular restricted three body problem (CRTBP) have found many families of solutions which do not have a lunar flyby, and even more families of solutions which do have a lunar flyby.[2,7] Some of these families exist so close to each other that they are equivalent in terms of practical implementation. Two families of solutions with a lunar flyby are shown in Fig. 1. Two families of solutions without a lunar flyby are shown in Fig. 2. Low-energy transfers such as these can form part of a transfer to any cislunar orbit – the examples shown arrive in an NRHO. Adding a targeted flyby increases the operational complexity but benefits the mission by reducing the launch vehicle C3 requirement, thus increasing the amount of delivered mass.

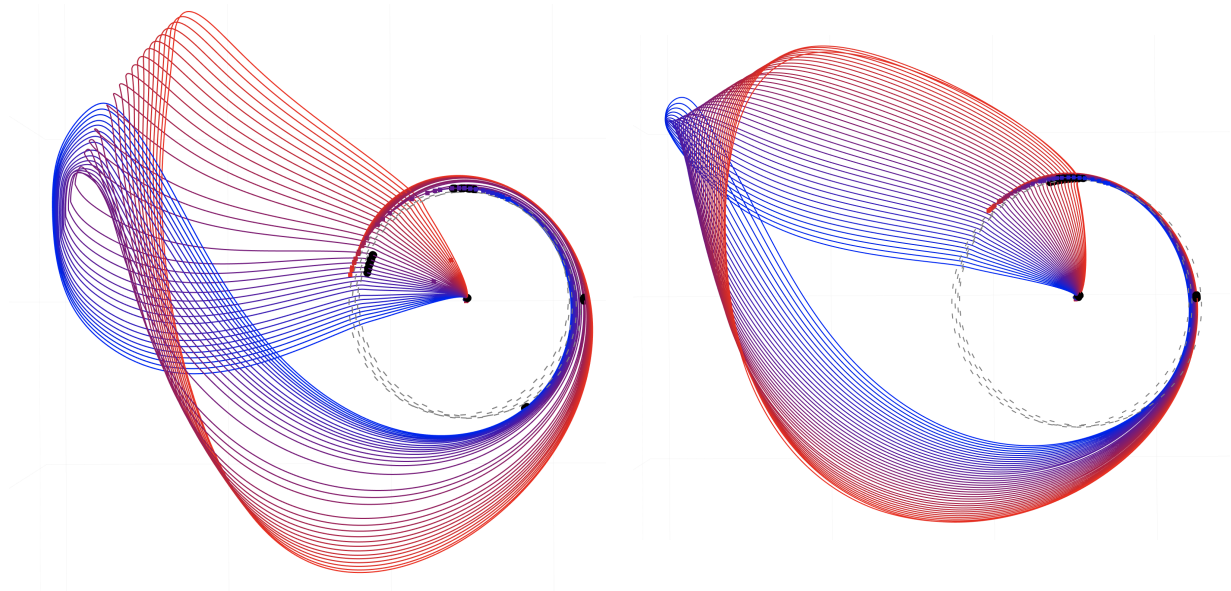

Figure 1. Example BLTs to NRHO with outbound lunar flyby. Each family is evaluated for 6 days to show the evolution of the family over time.

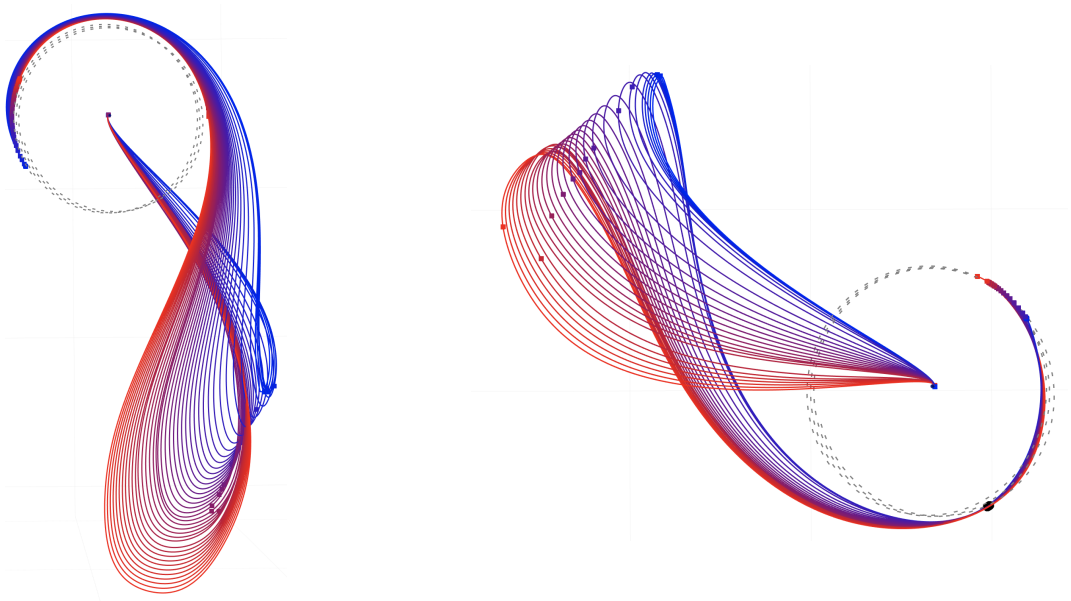

Figure 2. Example BLTs to NRHO without a targeted lunar flyby. Each family is evaluated over one month to show the evolution of the family over time.

II. Dynamics and Assumptions

Spacecraft dynamics in the current analysis are modeled in multiple high-fidelity, verified NASA tools: GMAT (the General Mission Analysis Tool, developed at Goddard Space Flight Center),[8] Monte (Mission Analysis, Operations, and Navigation Toolkit Environment, developed at the Jet Propulsion Laboratory),[9] and Copernicus trajectory design and optimization system (developed at Johnson Space Center).[10] In this analysis, GMAT and Copernicus are used to generate transfers for mission design and to represent the "truth" solution in orbit determination analyses. Force modeling includes:

- 32x32 spherical harmonics gravity field model of the Moon from the GRGM 900c model.
- Point masses of the Earth, Sun, and barycenters of all other planetary systems in the solar system, with states and gravitational parameters from the JPL DE430 ephemerides.[11]
- Solar radiation pressure, with a cannonball model and assuming mass of 14,000 kg, surface area of 23 m^2, and coefficient of reflectivity of 1.3. These are chosen to be representative of the Logistics Module for the Gateway.
- Relativistic correction.

For orbit determination analyses, the filter dynamics are slightly different from the "true" dynamics in order to represent realistic mis-modeling of gravitational and non-gravitational forces. The filter dynamics are implemented separately in Copernicus and Monte and include the following forces:

- 16x16 spherical harmonics gravity field model of the Moon from the GRGM 900c model.
- Point masses of the Earth, Sun, and barycenters of all other planetary systems in the solar system, with states and gravitational parameters from the JPL DE430 ephemerides,[11]
- Solar radiation pressure with a spherical spacecraft. Mass, surface area, and coefficient of reflectivity are initialized randomly with error according to the uncertainties given in Table 2.
- Relativistic correction.

Navigation is simulated separately in GMAT and in Monte. In both navigation simulations, the filter defines the dynamics in an Earth-centered J2000 inertial reference frame. The GMAT simulation uses a batch filter iterated until convergence. Convergence is defined as meeting the absolute and relative weighted RMS convergence criteria (0.01 and 0.001, respectively) and usually requires 3-5 iterations. GMAT's outer loop sigma editing (OLSE) is not used here because the simulated measurements are known to all be valid. In real operations, outlier measurements would be ignored to avoid incorporating bad data into the filter solution. The Monte simulation utilizes a U-D factorized covariance filter and uses stochastic accelerations on the order of 5×10^{-7} mm/s^2 updated every 8 hours to absorb dynamical mis-modeling.

In this analysis, a data arc is defined between maneuvers such as trans-lunar injection (TLI), trajectory correction maneuvers (TCMs), NRHO insertion maneuver (NIM), and insertion correction maneuvers (ICMs). Each data arc starts immediately following the previous maneuver and ends at the data cutoff 24 hours before the next maneuver (unless otherwise noted). Mimicking operational realism, this 24-hour cutoff period is meant to allow for the design, validation, and approval of a maneuver. Maneuvers are not estimated within the filters. Future analysis will model the maneuvers in the filter and also allow tracking passes during the 24 hours between data cutoff and the next maneuver (these data would be used to estimate the state for the subsequent data cutoff).

All analyses in this paper use three DSN ground stations, with a maximum of one ground station active at a time. The ground stations simulate a 35-m dish at the Madrid, Canberra, and Goldstone facilities. The Gateway is assumed to communicate with the DSN on X-band radio. Measurement noise in reality is dependent on the signal to noise ratio of the communication link, which is in turn dependent on many factors, such as the ground radio specifications, spacecraft radio specifications, and weather in Earth's ionosphere.[12] The measurement noise specified in Table 1 is chosen to be similar to the real measurement noise found from post-processing of navigation data from the ARTEMIS mission.[13] Measurement bias is modeled as fixed for all ground stations for all time.

All maneuvers are assumed to be impulsive changes in velocity (ΔV). Launch is not modeled; each simulation begins in a 100 km circular parking orbit around Earth with inclination of 28.5º, approximating the condition immediately after launch from Kennedy Space Center. The sources of uncertainty modeled here are presented in Table 1, and the error sources sampled for *a priori* state estimates are presented in Table 2.

Table 1. Assumed sources of uncertainty.

Error source	*Uncertainty (3σ)*
Mass uncertainty	3%
SRP area	30%
Coefficient of reflectivity	45%
Maneuver execution error	1.42 mm/s fixed, 1.5% proportional, 1 deg pointing
Measurement bias	7.5 m (range), 2.5 mm/s (range-rate)
Measurement noise	3 m (range), 1 mm/s (range-rate)

Table 2. Post-TLI a priori state error and covariance.

Estimated parameter	*3σ a priori state error relative to truth (applied once at start of simulation)*	*a priori covariance (re-initialized at the start of every data arc)*
Position in Earth-centered J2000	10 km	∞ km
Velocity in Earth-centered J2000	5 m/s	∞ m/s
Coefficient of reflectivity	45%	∞
Range measurement bias	1 m	∞
Range-rate measurement bias	1 mm/s	∞

III. "Trifecta" BLT Launch Opportunities

A previous BLT mission design analysis studied over 70,000 optimal BLTs to the 9:2 L_2 NRHO with outbound lunar flyby, with each BLT belonging to one of several distinct families.[6] The times of flight for these transfers vary from 16 to 25 weeks, creating a unique opportunity: a "trifecta" of launches, spaced one month apart, all rendezvous

with the Gateway in the NRHO at the same time or within one week. Such a trio of transfers could be beneficial for lunar human lander system architectures because the transfer element, descent element, and ascent element can each launch separately and arrive at the Gateway together. An example is shown in Figure 3.

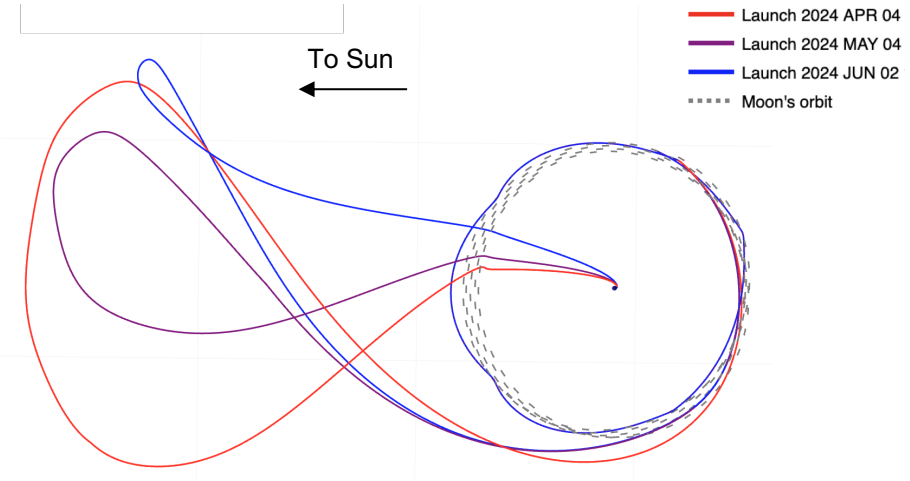

Figure 3. Example of a "trifecta" set of BLTs, shown from above in the Sun-Earth rotating reference frame with the Sun to the left.

The launch period for each of these BLTs is found to vary greatly depending on the particular geometry constraints of a given launch. Some families of BLTs typically have launch periods are as short as 1 day, while other families commonly have launch periods on the order of 10 days long. The launch periods can be extended by combining multiple families of solutions that exist near each other in the state space.[14] If one of the three launches were to miss its launch period, it would have to arrive on a different NRHO revolution and would typically be delayed by approximately 1-3 weeks. Figure 4 shows the frequency at which these synchronized launch opportunities exist. Each dot in the figure represents an available BLT with outbound lunar flyby with total deterministic ΔV under 100 m/s. Transfers are only indicated when the range of launch epochs spans at least two months.

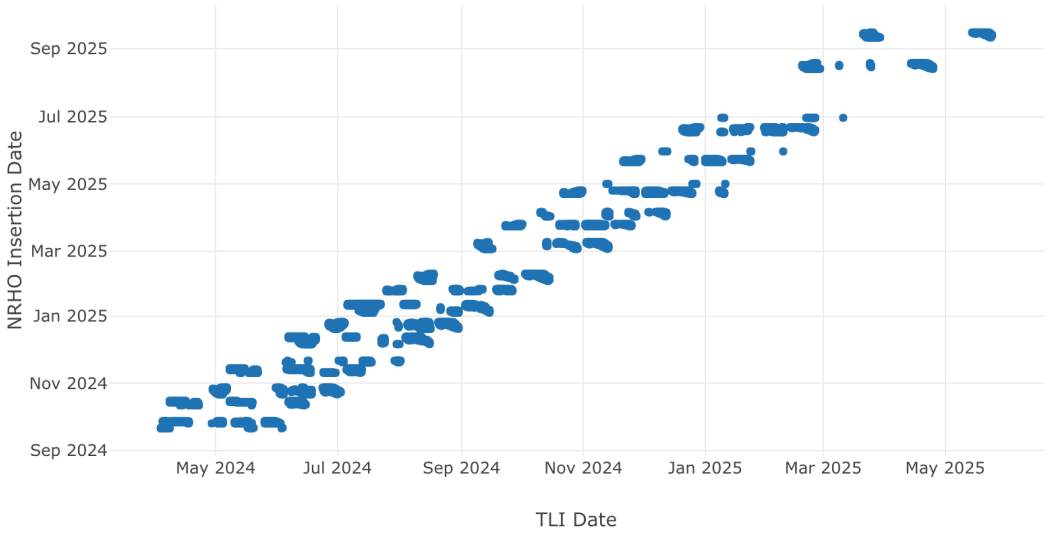

Figure 4. Opportunities for multiple launches with synchronized arrivals.

IV. Launch Injection Error

Three example nominal BLTs within the same launch period are used to study the effects of various sources of error on the ΔV required to actually fly such a transfer. These BLTs do not include a lunar flyby, and they represent the open, middle and close of a 10-day, representative launch period. Key parameters of the nominal transfers,

including deterministic ΔVs and times of flight, are described in Table 3. The launch period is centered on the lowest-cost transfer, with a total deterministic ΔV of 17.4 m/s. The open and close of the launch period require higher ΔV costs of about 41 m/s; the majority of the cost difference occurs at TCM-2 near apogee.

Table 3. Nominal ballistic lunar transfer, without lunar flyby.

	Launch Period		
	Open	Middle	Close
Deterministic TCM-2 ΔV	25.4 m/s	1.6 m/s	25.2 m/s
Nominal Insertion ΔV	15.8 m/s	15.8 m/s	15.9 m/s
Nominal Total ΔV	41.2 m/s	17.4 m/s	41.1 m/s
TLI Epoch	April 4, 2024 12:00:00 UTC	April 9, 2024 12:00:00 UTC	April 14, 2024 12:00:00 UTC
Time of flight	111.6 days	106.6 days	101.3 days

The transfer is assumed to have 5 TCM's, located notionally at each of the stars in Figure 5. TCM-2 is the only deterministic correction maneuver; the other TCMs offer opportunity for statistical corrections. Additional details on the timing and targets of each TCM appear in Table 4.

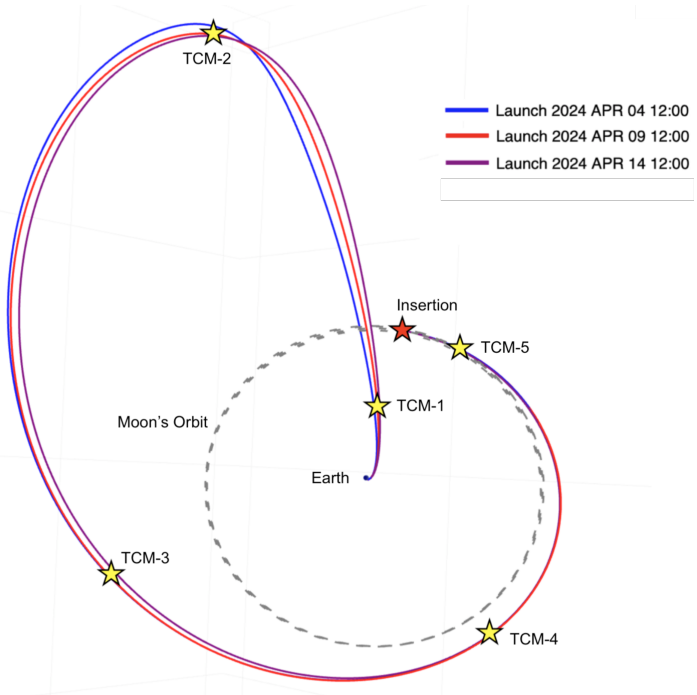

Figure 5. Approximate locations of each TCM for the example BLT studied, showing the open, middle, and close of the launch period. Plotted in the J2000 inertial reference frame.

Table 4. Description of Trajectory Correction Maneuver (TCM) timing and design.

Maneuver	*Timing*	*Design*
TCM-1	1 day after launch	Target position from back propagated nominal NRHO insertion at time of TCM-2 Minimize TCM-1 + TCM-2 ΔV
TCM-2	30 days after launch (or optimized)	Target position from back propagated nominal NRHO insertion at time of TCM-3 Minimize TCM-2 + TCM-3 ΔV
TCM-3	30 days before insertion	Target position from back propagated nominal NRHO insertion at time of TCM-4 Minimize TCM-3 + TCM-4 ΔV
TCM-4	10 days before insertion	Target position from back propagated nominal NRHO insertion at time of TCM-5 Minimize TCM-4 + TCM-5 ΔV
TCM-5	1 day before insertion	Target post-insertion maneuver state (start of NRHO) Minimize TCM-5 + Insertion ΔV

The nominal transfer is nearly ballistic, with a deterministic TCM-2 ΔV of 1.6 m/s and a total deterministic ΔV of 17.4 m/s. The following set of analyses examine various contributors to the statistical ΔV, beginning with the launch injection state error. Typical launch errors (based approximately on various launch vehicles the authors are familiar with) are considered, with 3σ C3 error of 0.1 km^2/s^2 and 3σ angle error of 1 degree. Here, the angle error is represented as an error in argument of perigee (AoP), right ascension of ascending node (RAAN), and inclination. Figure 6 shows the contribution of each of these sources of error to the total TCM ΔV. The open, middle, and close of a notional launch period are shown. At the open and close of this launch period, the nominal ΔV is approximately 30 m/s. It is clear that the most significant error source is the launch C3. The middle of the launch period has ΔV between 1.6 m/s and 30 m/s. The open and close of the launch period have ΔV between 30 m/s and 55 m/s. In this figure, TCM-1 takes place 24 hours after trans-lunar injection (TLI).

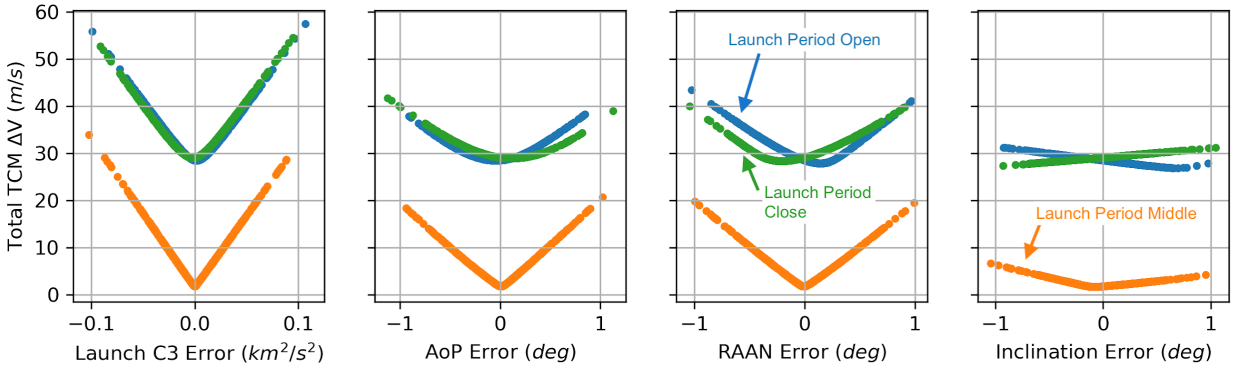

Figure 6. Total TCM ΔV as a function of launch error, with errors sampled individually.

All sources of error (launch state, orbit determination, and maneuver execution) are then sampled together to understand the effect of their cross-coupling. The results appear in Figure 7, with the TCM-1 ΔV plotted as a function of launch C3 error and angle error, for the nominal launch epoch. In this figure, it is clear once more that the TLI error drives the TCM-1 ΔV. When the errors are considered together, the TCM-1 ΔV can exceed 50 m/s. The launch vehicle

injection error can, in some cases, be the largest contributor to the total spacecraft ΔV requirements, so it is important to understand this effect.

The timing of TCM-1 is varied between 12 hours and 96 hours after TLI. The earlier TCM-1 takes place, the lower the total ΔV (errors can be corrected while still close to Earth). Practical navigation and operational constraints limit the time required between TLI and TCM-1.

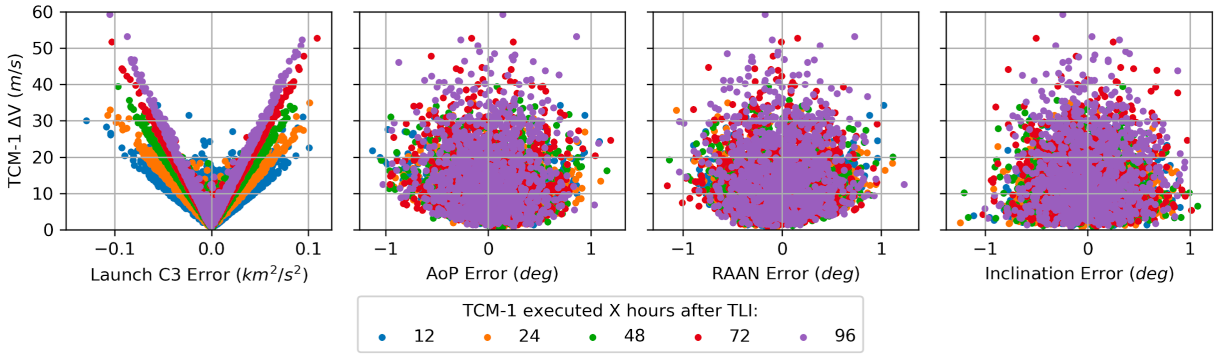

Figure 7. TCM-1 ΔV as a function of launch error and TCM-1 timing, with errors sampled together.

V. Navigation Requirements Analysis

Continuing with the same nominal transfer, a navigation analysis is performed. Requirements on BLT navigation accuracy are considered by exploring the relationship between navigation uncertainty and TCM ΔV, and by exploring the relationship between navigation uncertainty and NRHO insertion accuracy. A navigation requirements simulation is performed with the following errors modeled:

- Launch injection,
- Navigation error (found by randomly perturbing the truth according to an assumed distribution for navigation uncertainty), and
- Maneuver execution error (using the Gates model [15] with fixed and proportional pointing errors and fixed and proportional magnitude errors).

For each trade, a Monte Carlo analysis of 500 trials each is performed. In each trial, the BLT is built up one maneuver at a time. Each TCM is designed according to the logic described in Table 4, above. Essentially, each TCM is considered as the first of two maneuvers to retarget the nominal transfer. In some trials, the NRHO insertion maneuver (NIM) design is allowed to change during each TCM design, and in others, the NIM is held fixed until the TCM-5 design. TCM-5 and NIM are designed together, so the NIM design is fixed at the TCM-5 data cutoff epoch (two days before NIM execution).

A 24-hour data cutoff is enforced for each TCM. To simulate this cutoff, the specified navigation error is sampled at the data cutoff epoch. The sample (with error) is then propagated to the maneuver execution epoch and executed with random errors according to the Gates model. The TCM is designed based on the truth trajectory and executed by the sample with simulated OD error — which becomes the new truth trajectory going forward. TCM-1 occurs shortly after launch, so the data cutoff is reduced to 8 hours before the maneuver execution epoch in that case.

A. TCM placement trades.

There is no obvious ideal number of TCMs or timing of TCMs. Some things are clear, though, from experience. For instance, it is clear from the analysis of the launch error and TCM-1 that TCM-1 should be performed as soon as it is feasible. TCM-2 (located nominally at apogee) is the only one designed to have a deterministic component. Using that deterministic maneuver to also clean up errors is beneficial because the vector addition of the deterministic and stochastic components is less than or equal to the magnitude of the two components separately. Early analysis of BLTs shows that the transfers are highly sensitive to the NRHO insertion state, so it is reasonable to add a clean-up maneuver shortly before NRHO insertion — TCM-5 in this analysis.

The real question, then, is how many TCMs should take place between TCM-2 and the maneuver immediately before NRHO insertion. The results presented here show that inserting two TCMs between the second and final maneuvers is preferable to having just one TCM in that segment of the trajectory. The number of TCMs thus comes out to 5, with the approximate timing discussed above in Table 5. Consideration of additional TCMs is left to future work. The results of an analysis appear in Tables 7-9 to consider the optimal timing of TCM-3 relative to the NRHO insertion, for the open, middle, and close of the launch period. Each of these three tables shows the mean and 99th

percentile ΔV (ΔV99) for each TCM individually and the total of all TCMs. Each column in each table represents a Monte Carlo analysis of 500 random samples. For these results, the 3σ navigation error is assumed to be 3/30/30 km and 3/30/30 cm/s (radial/transverse/normal directions), and the 3σ maneuver execution error is assumed to have a 3 cm/s fixed error component and 3% proportional error components in both magnitude and pointing. Later sections of this analysis consider the effects of changing the navigation and maneuver execution errors.

Table 5. TCM-3 timing study for the beginning of the launch period.

	TCM-3 Execution Time (days before NIM)					
	No TCM-3		20 days	30 days	40 days	50 days
Maneuver	μ (m/s)	ΔV99 (m/s)				
TCM-1	11.20	27.67	11.65 / 27.50	11.31 / 28.03	11.54 / 29.99	11.53 / 29.87
TCM-2	25.33	27.92	25.33 / 27.54	25.39 / 28.04	25.39 / 27.62	25.43 / 27.95
TCM-3	-	-	9.04 / 27.44	3.70 / 12.25	1.77 / 5.67	1.02 / 3.01
TCM-4	25.13	80.09	2.04 / 7.82	0.96 / 3.69	1.22 / 3.41	1.95 / 5.76
TCM-5	25.64	84.75	5.08 / 16.45	5.47 / 15.07	5.70 / 15.39	5.945 / 15.44
Total	87.29	203.35	53.14 / 85.29	46.82 / 68.48	45.61 / 65.36	45.88 / 64.15

Table 6. TCM-3 timing study for the middle of the launch period.

	TCM-3 Execution Time (days before NIM)					
	No TCM-3		20 days	30 days	40 days	50 days
Maneuver	μ (m/s)	ΔV99 (m/s)				
TCM-1	11.37	29.25	11.48 / 28.50	11.43 / 28.20	11.53 / 29.23	11.54 / 28.44
TCM-2	2.41	5.14	2.36 / 5.88	2.41 / 5.92	2.45 / 5.60	2.39 / 5.80
TCM-3	--	--	1.94 / 5.98	0.82 / 2.40	0.46 / 1.25	0.37 / 1.16
TCM-4	5.23	16.94	0.46 / 1.16	0.53 / 1.59	1.05 / 3.19	1.92 / 6.34
TCM-5	7.88	23.70	4.95 / 16.14	5.27 / 17.09	5.61 / 15.32	6.06 / 18.25
Total	26.89	57.21	21.19 / 42.84	20.47 / 41.79	21.10 / 43.54	22.27 / 45.01

Table 7. TCM-3 timing study for the end of the launch period.

Maneuver	TCM-3 Execution Time (days before NIM)					
	No TCM-3		20 days	30 days	40 days	50 days
	μ (m/s)	ΔV99 (m/s)				
TCM-1	11.20	27.38	11.33 / 28.18	11.29 / 28.66	11.37 / 28.37	11.47 / 28.88
TCM-2	25.12	28.61	25.12 / 28.37	25.16 / 29.37	25.16 / 28.40	25.15 / 28.64
TCM-3	--	--	6.18 / 19.58	2.32 / 7.95	1.23 / 3.57	0.77 / 2.11
TCM-4	17.14	56.07	1.24 / 5.20	0.72 / 2.23	1.19 / 3.54	1.96 / 6.32
TCM-5	18.66	62.95	4.89 / 15.60	5.18 / 15.84	5.84 / 16.57	5.87 / 16.66
Total	72.12	154.28	48.76 / 73.95	44.66 / 64.91	44.77 / 63.76	45.23 / 67.31

From this analysis, the optimal timing of TCM-3 can be selected for each case. At the beginning of the launch period, the lowest ΔV99 is achieved by performing TCM-3 50 days before NIM. This is likely because TCM-2 has a significant deterministic cost (ΔV99 of 28 m/s), so TCM-3 acts as a cleanup maneuver for TCM-2. In the middle of the launch period, the optimal timing of TCM-3 is at 30 days before NIM. In this case, TCM-2 is small (ΔV99 of 6 m/s), so it is preferable to have TCM-3 later in the transfer so that it is more evenly spaced between TCM-2 and TCM-4. At the end of the launch period, the optimal timing (minimum total ΔV99) of TCM-3 is at 40 days before NIM, similar to the beginning of the launch period.

B. Effect of TCM-5 execution error on NRHO insertion error

For this analysis, the NIM is assumed to be performed at perilune, at which point the orbital energy change can be accomplished for the minimum ΔV. There is a trade-off between maneuver efficiency and the accuracy of the achieved insertion state. The closer NIM is performed to perilune, the smaller the maneuver can be because of the Oberth effect [16]. However, the Oberth effect also means that orbit determination errors and maneuver execution errors are magnified.

A previous analysis found that the deterministic ΔV for NRHO insertion can be 10-30 m/s lower when insertion is performed near perilune than when performed 24 hours later [6]. If the cleanup maneuver(s) require less ΔV than the ΔV savings from inserting at perilune, then it is better to choose to insert at perilune. A parallel study explores the insertion correction maneuver strategy and ΔV requirements[17], with the core finding that the clean-up ΔV is a function of the state error immediately after NIM. The present study examines the effect that maneuver execution error and OD knowledge before NIM have on the state error immediately after NIM. Combining the results of these two studies, reveals that, for realistic tracking schedules and maneuver execution errors, the total ΔV required for insertion at perilune and clean-up maneuvers is smaller than the ΔV required for insertion 24 hours after perilune.

Figure 8 shows the achieved NRHO insertion state error mapped to perilune, as a function of the TCM-5 maneuver execution error. The NRHO insertion state error is represented in the Moon-centered, Earth-Moon rotating frame, while the maneuver execution errors are represented in an Earth-centered inertial frame. Figure 9 shows the same insertion error as a function of the state error immediately after TCM-5, which is analogous to the orbit determination error. From these figures, the most significant contributor to the insertion error is the velocity state error after TCM-5. This suggests that reducing the OD uncertainty is the most effective way to reduce the NRHO insertion error.

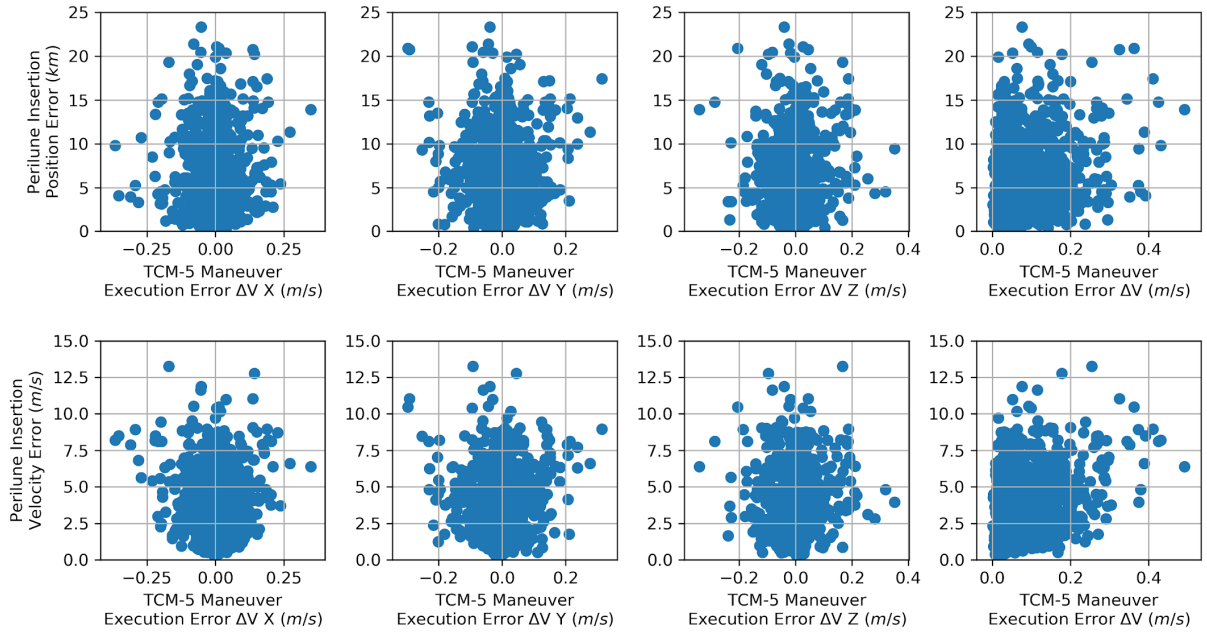

Figure 8. TCM-5 execution error vs. NRHO insertion error.

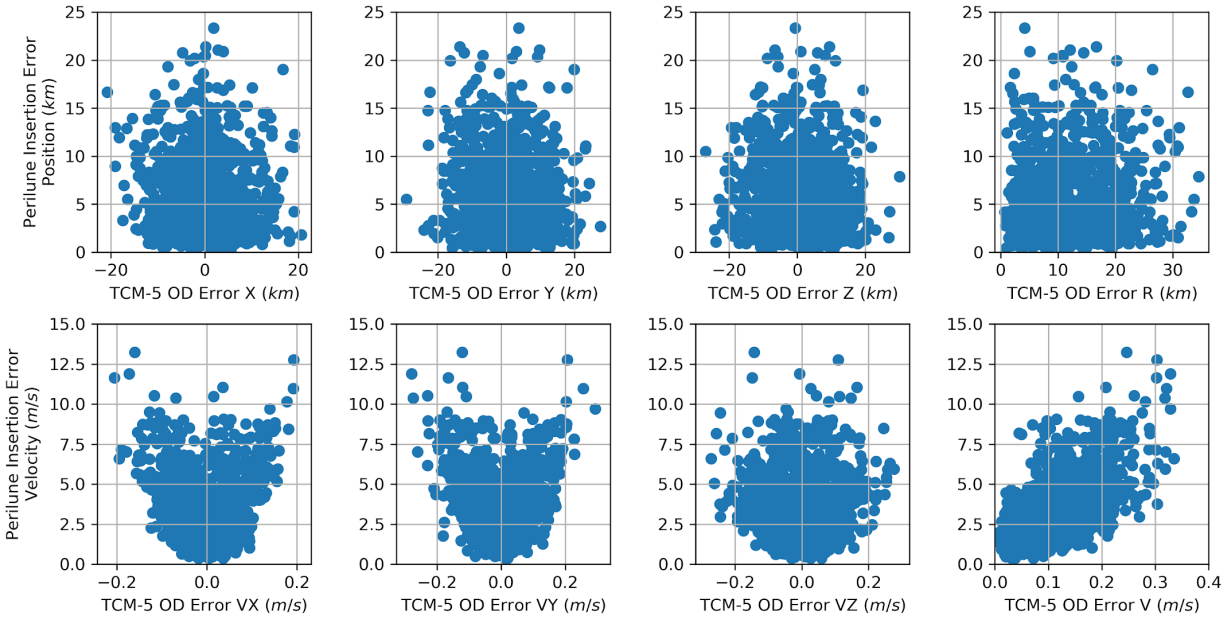

Figure 9. State error immediately after TCM-5 vs. NRHO insertion accuracy.

The present study, in combination with the partner paper[17], finds that given reasonable OD knowledge before NIM (so that TCM-5 and NIM can be designed accurately) and after NIM (so that cleanup maneuvers can be executed within the first revolution of the NRHO), executing NIM at perilune is the most fuel efficient option.

C. Effect of OD uncertainty on future TCMs, total ΔV, and insertion accuracy

The next analysis considers the effect of assumed OD uncertainty on the ΔV for each TCM, NIM, and the mission total, as well as the effect on the NRHO insertion state. Two cases are examined: one with a high assumed OD uncertainty, and one with a low assumed OD uncertainty. The high uncertainty case uses 3σ OD errors of 3/30/30 km and 3/30/30 cm/s in the radial/transverse/normal (RTN) directions of a frame defined by the spacecraft motion relative

to Earth. The low uncertainty case uses 3σ OD errors of 0.3/3/3 km and 0.3/3/3 cm/s in the RTN frame. A Monte Carlo analysis was run with 1,000 samples each for the high- and low-error cases. Figures 10-11 show the transfer ΔV requirements for the high- and low-error cases, respectively, broken down by the ΔV for each maneuver and the total ΔV.

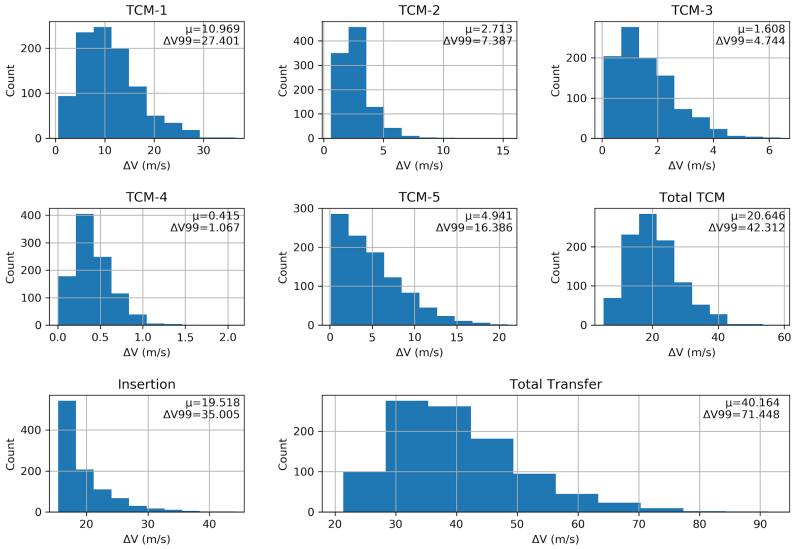

Figure 10. BLT transfer ΔV requirements, with 3σ orbit determination errors of 3/30/30 km, 3/30/30 cm/s in RTN frame.

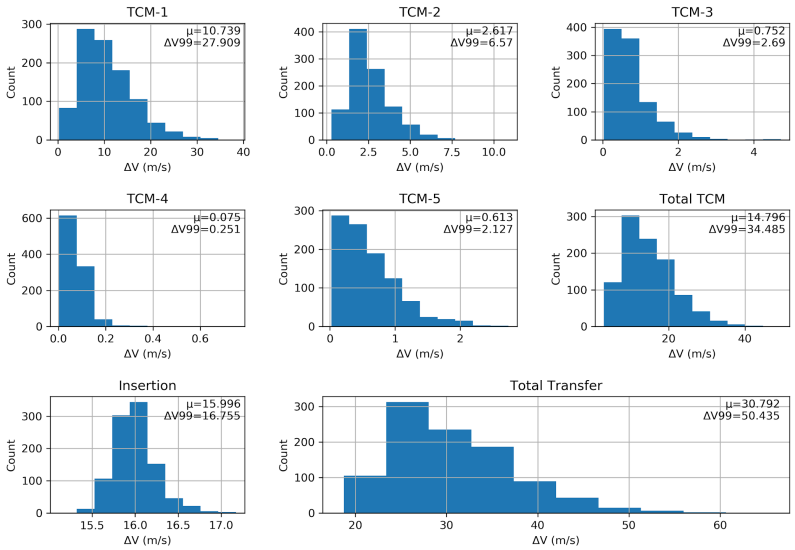

Figure 11. BLT transfer ΔV requirements, with 3σ orbit determination errors of 0.3/3/3 km, 0.3/3/3 cm/s in RTN frame.

As a result of the different geometry for each maneuver relative to the Earth, Moon, and Sun, some maneuvers are more sensitive than others. TCM-1 is 27-28 m/s regardless of the OD error because TCM-1 is mainly determined by the launch error. For this transfer, TCM-2 is small ($\Delta V99$ of approximately 7 m/s) regardless of the OD error, as the main contributor to TCM-2 ΔV is TCM-1 execution error. TCM-5 is different in that it varies substantially as a function of OD error — the high error case has a $\Delta V99$ of 16 m/s, and the low error case has a $\Delta V99$ of 2 m/s. This insight is useful because it informs where additional ground station tracking is most beneficial. The total transfer $\Delta V99$ is 71 m/s for the high error case and 50 m/s for the low error case. In comparison with the nominal, error-free BLT transfer cost of 17 m/s, the errors added approximately 30-50 m/s of statistical ΔV to cover 99% of Monte Carlo trials.

An additional case with even lower error is run to assess if the ΔV continues to improve. It is found that for errors below the 0.3/3/3 km, 0.3/3/3 cm/s case, the performance does not improve any further. At this point, the maneuver execution errors are the dominating factor.

Figure 12 shows the NRHO insertion error mapped to perilune for the large assumed OD uncertainty, and Figure 13 shows the same error for the small assumed OD uncertainty. Reducing the assumed OD uncertainty by a factor of 10 produces nearly the same amount of reduction in the achieved insertion state, confirming that the OD error is indeed the primary contributor to the insertion accuracy. Given that the NRHO is sensitive enough that a 15-20 m/s maneuver is sufficient to insert or depart the NRHO within a single revolution, the up-to-10 m/s achieved velocity error for the large OD error case is not acceptable. The tracking schedule must be chosen such that something similar to the small assumed OD error is achieved for the state estimate prior to TCM-5.

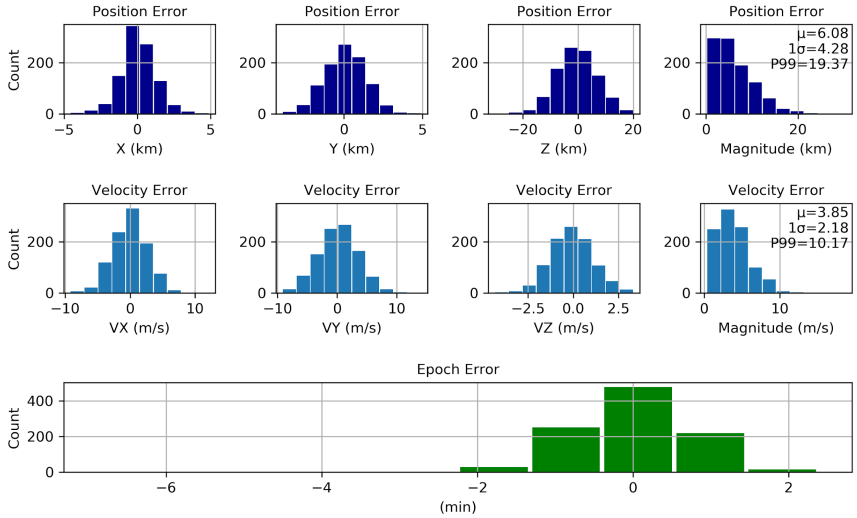

Figure 12. Perilune insertion state error in Earth-Moon rotating frame with 3σ orbit determination errors of 3/30/30 km, 3/30/30 cm/s in RTN frame.

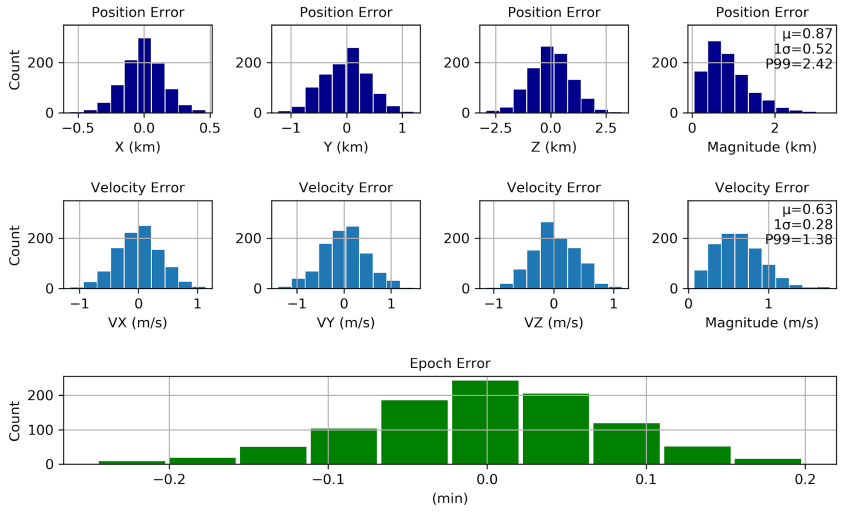

Figure 13. Perilune insertion state error in Earth-Moon rotating frame with 3σ orbit determination errors of 0.3/3/3 km, 0.3/3/3 cm/s in RTN frame.

Figure 14 shows the relationship between the OD errors at one TCM and the ΔV required at the next TCM. It is clear that the velocity component of the OD uncertainty is a large driver for the magnitude of the subsequent TCM. This analysis also suggests a way to reduce the statistical ΔV for a transfer: strategic use of ground tracking to reduce the OD error at key points. For instance, adding extra tracking passes (and thus, reducing the state error) before TCM-4 could reduce the ΔV for TCM-5 by as much as 18 m/s.

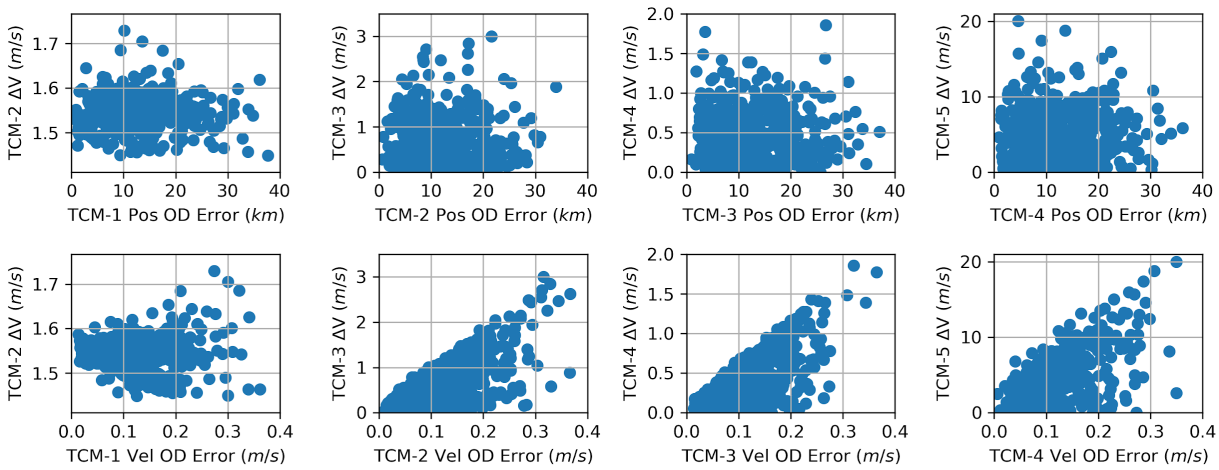

Figure 14. Relationship between OD error at each TCM and the ΔV to recover at the next TCM.

VI. BLT Navigation with Simulated Orbit Determination

Simulated orbit determination is performed in Monte using the U-D factorized covariance filter. The dynamics for the truth and navigation spacecraft as well as the assumptions about DSN noise are described in Section II. To mimic operational realism, the truth spacecraft is propagated outside of Monte entirely. The simulated measurements are generated in Monte, but the filter never comes into contact with the raw truth states. For this analysis, the following tracking cadences are evaluated:

- Continuous
- 8 hours per pass, 7 passes per week
- 8 hours per pass, 3 passes per week
- 8 hours per pass, 2 passes per week
- 2 hours per pass, 7 passes per week
- 2 hours per pass, 3 passes per week
- 2 hours per pass, 2 passes per week

The state uncertainties at each TCM are calculated for each of the proposed tracking schedules. These uncertainties are estimated by the covariance of a U-D factorized covariance filter. For each tracking leg, the a priori state estimate is taken as the previous leg's final state perturbed by the 3-sigma covariance, and the initial covariance is inflated by a factor of ten over the previous leg's ending covariance. The resulting position uncertainty for each tracking cadence and each leg is shown in Fig. 15, and velocity uncertainty is shown in Fig. 16. The raw results are located in Tables 8-9.

Table 8: One-sigma position uncertainty (km) as estimated by filter

Cadence / TCM	TCM-1	TCM-2	TCM-3	TCM-4	TCM-5
Continuous	1.03E-01	2.17E-02	1.74E-02	1.20E-02	1.17E-02
8 hr/7 per week	N/A	1.03E-01	7.07E-02	3.72E-02	1.13E-01
8 hr/3 per week	N/A	1.93E-01	1.07E-01	5.94E-02	3.20E-01
8 hr/2 per week	N/A	2.44E-01	1.35E-01	1.21E-01	6.12E-01
2 hr/7 per week	N/A	1.32E-01	1.19E-01	4.33E-02	9.88E-02
2 hr/3 per week	N/A	3.27E-01	2.80E-01	9.43E-02	3.17E-01
2 hr/2 per week	N/A	6.35E-01	4.11E-01	1.94E-01	4.91E-01

Table 9: One-sigma velocity uncertainty (m/s) as estimated by filter

Cadence / TCM	TCM-1	TCM-2	TCM-3	TCM-4	TCM-5
Continuous	1.75E-03	1.07E-04	9.90E-05	9.00E-05	9.80E-05
8 hr/7 per week	N/A	1.59E-04	1.48E-04	1.39E-04	5.55E-04
8 hr/3 per week	N/A	1.92E-04	1.80E-04	1.81E-04	1.59E-03
8 hr/2 per week	N/A	2.18E-04	2.01E-04	3.42E-04	3.22E-03
2 hr/7 per week	N/A	1.78E-04	1.67E-04	1.46E-04	4.67E-04
2 hr/3 per week	N/A	2.18E-04	2.21E-04	2.83E-04	1.47E-03
2 hr/2 per week	N/A	2.50E-04	2.76E-04	4.62E-04	2.33E-03

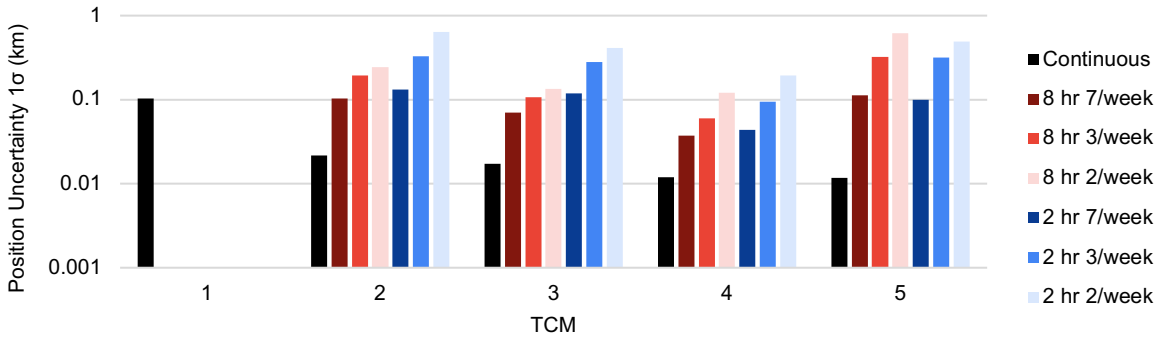

Figure 15. Position 1-sigma uncertainty at each TCM for various tracking cadences.

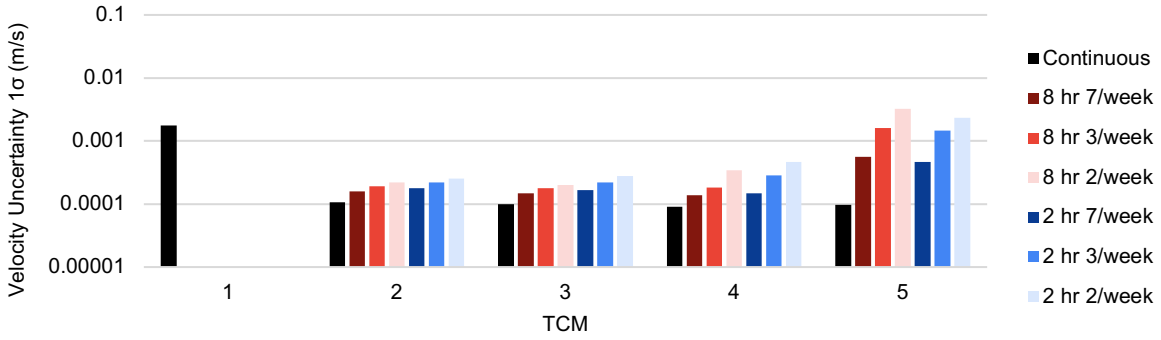

Figure 16. Velocity 1-sigma uncertainty at each TCM for various tracking cadences.

For these runs, perhaps the most surprising result is the large position and velocity uncertainty at TCM-1, even though the only analyzed cadence is continuous tracking. This is primarily a result of the relatively high uncertainty at TLI, which is only 24 hours before TCM-1. The data cutoff for the TLI - TCM-1 leg is at 8 hours prior to TCM-1, but for this filter, 16 hours of continuous tracking is not enough time to shrink the covariance to a magnitude similar to other TCMs. Future studies will examine the achievable state uncertainty at TCM-1 as a function of time after TLI and as a function of the a priori state uncertainty (which varies depending on the launch vehicle).

Figure 17 illustrates an important trend: the way the instantaneous position and velocity uncertainty grows between tracking passes and shrinks quickly during each tracking pass. In this example, there is a 6-hour pass three times per week for the entire transfer. The TCMs for this BLT are small, so the filter is able to build them into the

dynamics purely with stochastic acceleration. A more accurate solution could be found by also estimating the maneuvers within the filter.

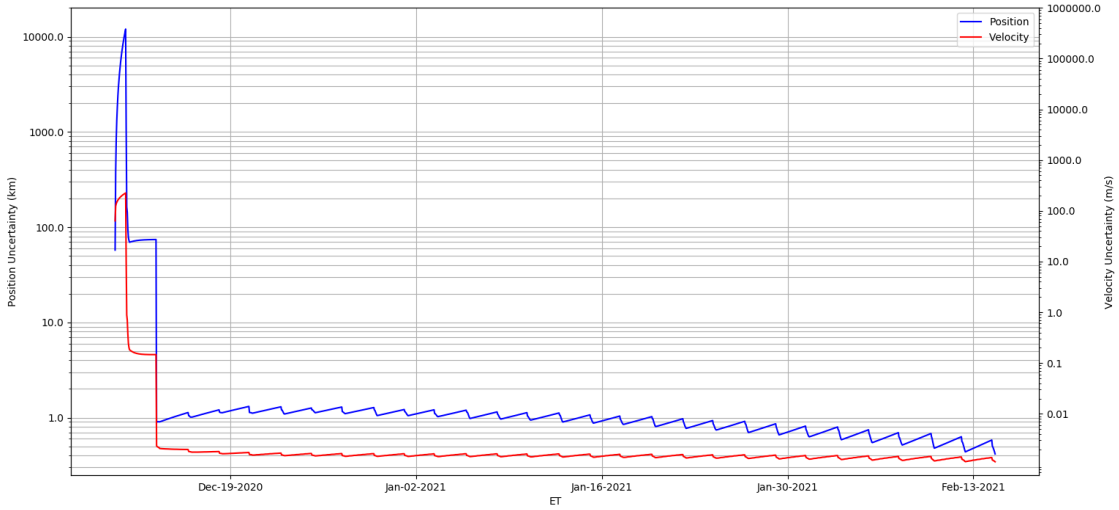

Figure 17. Position and velocity 1-sigma uncertainty over an entire BLT. *TCMs are modeled purely by stochastic acceleration in the filter.*

In order to verify the accuracy of the covariance estimate, a Monte Carlo analysis is run with simulated measurements. For each of the transfer legs, 100 random samples of simulated navigation are performed. Each sample uses different simulated measurements with the same tracking schedule. The post-TLI *a priori* states and covariances are generated based on the uncertainties in Table 2. The *a priori* state guesses and covariances for all future legs are generated based on the covariance of the previous leg at the given tracking schedule. The *a priori* state is randomly sampled as a function of the previous leg's covariance, and the previous covariance is inflated by a factor of ten at each maneuver. Then, the state estimated by the filter at the next TCM is compared to the truth state at the next TCM, and the errors recorded. The means and standard deviations of the distributions of errors for each TCM and each tracking cadence appear in Tables 10-11, and Figures 18-21.

Table 10: Mean and standard deviation of position estimate error vectors (km) from Monte Carlo results

Cadence / TCM	TCM-1	TCM-2	TCM-3	TCM-4	TCM-5
Continuous	$\mu = 1.91*10^{-1}$ $\sigma = 1.40*10^{0}$	$\mu = 2.52*10^{-3}$ $\sigma = 9.91*10^{-3}$	$\mu = 3.41*10^{-3}$ $\sigma = 6.73*10^{-3}$	$\mu = 1.58*10^{-3}$ $\sigma = 4.32*10^{-3}$	$\mu = 3.69*10^{-4}$ $\sigma = 3.41*10^{-3}$
8 hr/7 per week	N/A	$\mu = 1.65*10^{-2}$ $\sigma = 4.08*10^{-2}$	$\mu = 3.18*10^{-3}$ $\sigma = 2.40*10^{-2}$	$\mu = 3.85*10^{-3}$ $\sigma = 8.51*10^{-3}$	$\mu = 4.74*10^{-3}$ $\sigma = 4.76*10^{-2}$
8 hr/3 per week	N/A	$\mu = 2.86*10^{-2}$ $\sigma = 8.62*10^{-2}$	$\mu = 6.77*10^{-3}$ $\sigma = 2.83*10^{-2}$	$\mu = 6.93*10^{-3}$ $\sigma = 1.78*10^{-2}$	$\mu = 8.38*10^{-3}$ $\sigma = 1.43*10^{-1}$
8 hr/2 per week	N/A	$\mu = 3.72*10^{-2}$ $\sigma = 1.09*10^{-1}$	$\mu = 1.07*10^{-2}$ $\sigma = 3.53*10^{-2}$	$\mu = 1.38*10^{-2}$ $\sigma = 3.94*10^{-2}$	$\mu = 8.84*10^{-3}$ $\sigma = 3.07*10^{-1}$
2 hr/7 per week	N/A	$\mu = 2.02*10^{-2}$ $\sigma = 2.74*10^{-2}$	$\mu = 4.04*10^{-3}$ $\sigma = 2.60*10^{-2}$	$\mu = 4.19*10^{-3}$ $\sigma = 1.13*10^{-2}$	$\mu = 1.43*10^{-3}$ $\sigma = 4.91*10^{-2}$
2 hr/3 per week	N/A	$\mu = 4.08*10^{-2}$ $\sigma = 1.40*10^{-1}$	$\mu = 9.32*10^{-3}$ $\sigma = 7.70*10^{-2}$	$\mu = 1.07*10^{-2}$ $\sigma = 2.95*10^{-2}$	$\mu = 2.86*10^{-3}$ $\sigma = 1.70*10^{-1}$
2 hr/2 per week	N/A	$\mu = 3.08*10^{-2}$ $\sigma = 1.98*10^{-1}$	$\mu = 2.14*10^{-2}$ $\sigma = 1.65*10^{-1}$	$\mu = 1.85*10^{-2}$ $\sigma = 7.79*10^{-2}$	$\mu = 9.99*10^{-3}$ $\sigma = 2.50*10^{-1}$

Table 11: Mean and standard deviation of velocity estimate error vectors (m/s) from Monte Carlo results

Cadence / TCM	TCM-1	TCM-2	TCM-3	TCM-4	TCM-5
Continuous	$\mu = 2.58*10^{-3}$ $\sigma = 1.89*10^{-2}$	$\mu = 1.39*10^{-5}$ $\sigma = 2.83*10^{-5}$	$\mu = 3.87*10^{-6}$ $\sigma = 1.62*10^{-5}$	$\mu = 1.30*10^{-5}$ $\sigma = 1.96*10^{-5}$	$\mu = 4.51*10^{-6}$ $\sigma = 2.44*10^{-5}$
8 hr/7 per week	N/A	$\mu = 3.09*10^{-5}$ $\sigma = 2.78*10^{-5}$	$\mu = 1.43*10^{-5}$ $\sigma = 3.09*10^{-5}$	$\mu = 1.76*10^{-5}$ $\sigma = 2.71*10^{-5}$	$\mu = 2.91*10^{-5}$ $\sigma = 2.66*10^{-4}$
8 hr/3 per week	N/A	$\mu = 4.56*10^{-5}$ $\sigma = 3.46*10^{-5}$	$\mu = 1.94*10^{-5}$ $\sigma = 1.77*10^{-5}$	$\mu = 2.41*10^{-5}$ $\sigma = 4.42*10^{-5}$	$\mu = 4.55*10^{-5}$ $\sigma = 8.23*10^{-4}$
8 hr/2 per week	N/A	$\mu = 5.31*10^{-5}$ $\sigma = 2.88*10^{-5}$	$\mu = 2.36*10^{-5}$ $\sigma = 3.26*10^{-5}$	$\mu = 4.59*10^{-5}$ $\sigma = 1.17*10^{-4}$	$\mu = 2.41*10^{-5}$ $\sigma = 1.77*10^{-3}$
2 hr/7 per week	N/A	$\mu = 3.67*10^{-5}$ $\sigma = 3.13*10^{-5}$	$\mu = 1.62*10^{-5}$ $\sigma = 2.94*10^{-5}$	$\mu = 1.82*10^{-5}$ $\sigma = 3.42*10^{-5}$	$\mu = 4.45*10^{-6}$ $\sigma = 2.23*10^{-4}$
2 hr/3 per week	N/A	$\mu = 5.48*10^{-5}$ $\sigma = 5.26*10^{-5}$	$\mu = 2.16*10^{-5}$ $\sigma = 3.52*10^{-5}$	$\mu = 3.57*10^{-5}$ $\sigma = 9.41*10^{-5}$	$\mu = 8.17*10^{-6}$ $\sigma = 7.87*10^{-4}$
2 hr/2 per week	N/A	$\mu = 5.61*10^{-5}$ $\sigma = 6.87*10^{-5}$	$\mu = 2.44*10^{-5}$ $\sigma = 5.07*10^{-5}$	$\mu = 5.42*10^{-5}$ $\sigma = 1.83*10^{-4}$	$\mu = 4.73*10^{-5}$ $\sigma = 1.22*10^{-3}$

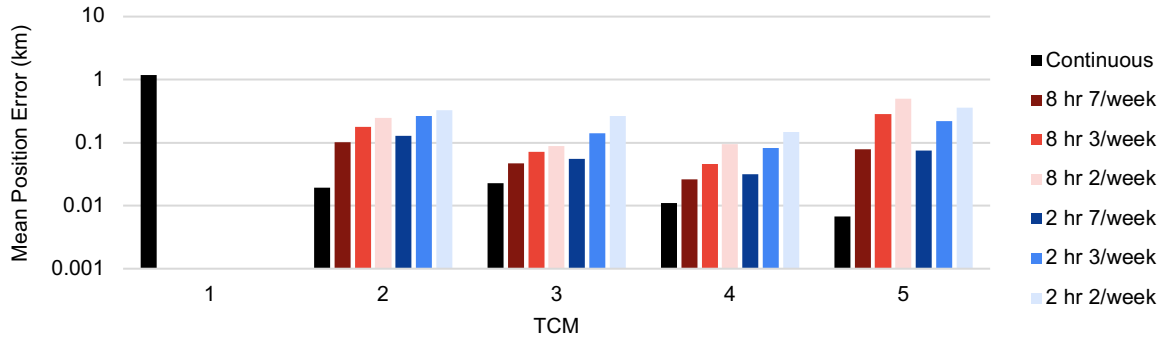

Figure 18. Mean of position state estimate error magnitudes at each TCM for various tracking cadences.

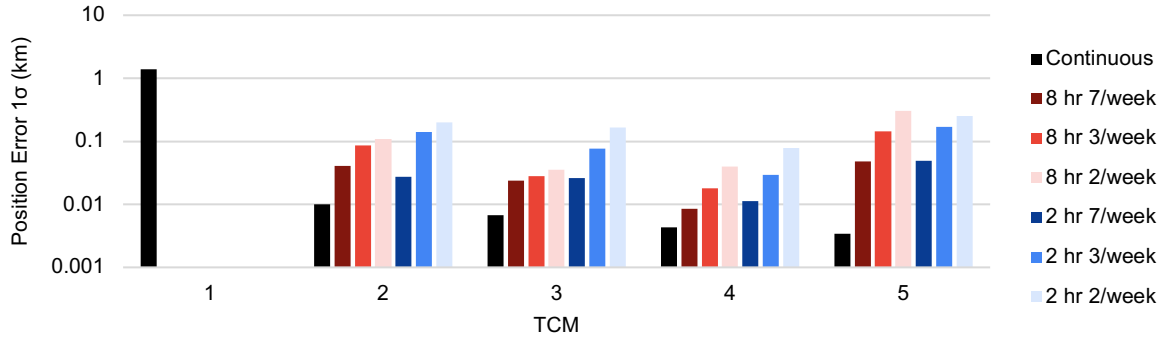

Figure 19. Standard deviation of position state estimate errors at each TCM for various tracking cadences.

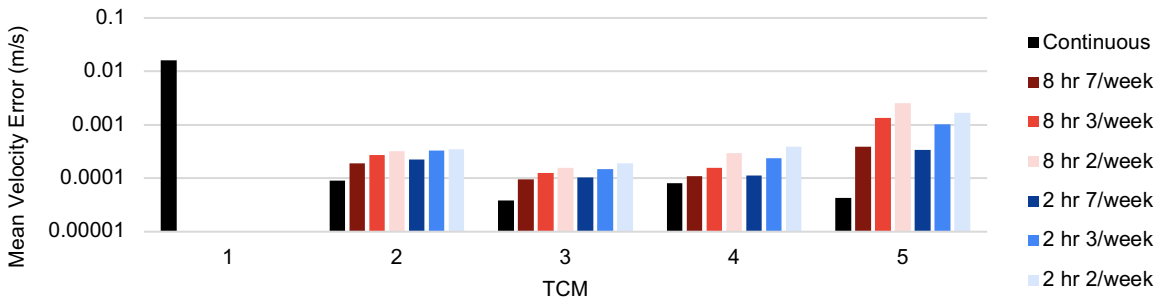

Figure 20. Mean of velocity state estimate error magnitudes at each TCM for various tracking cadences.

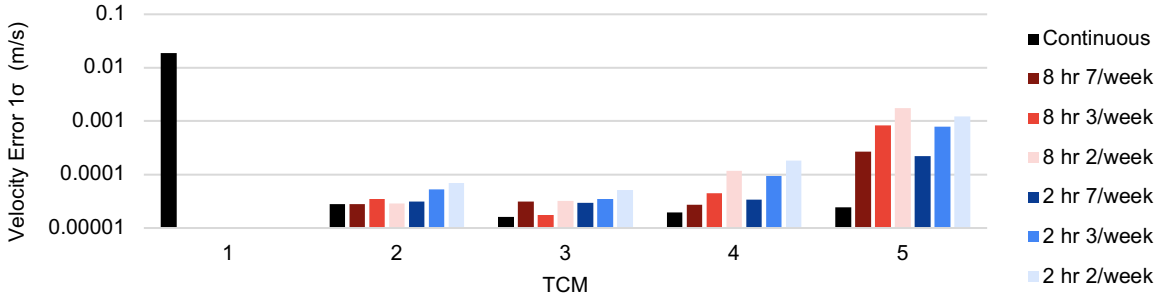

Figure 21. Standard deviation of velocity state estimate errors at each TCM for various tracking cadences.

A sample distribution of the position and velocity filter uncertainties against Monte Carlo position means is shown in Figure 22. It is clear that for some sections of the transfer, the filter did not converge on the correct solution. The dotted line indicates the point at which the mean of the error magnitudes is equal to the expected distribution from the covariance analysis. Points at or below the dotted line represent Monte Carlo analyses with reliable state estimates. Points above the dotted line represent Monte Carlo analyses where the filter saturated and converged on the wrong solution, which is most clear with the state estimate immediately before TCM-1. Various strategies have been identified to improve the filter performance: break the long data arcs into multiple, short arcs; tune the stochastic acceleration; and "consider" additional parameters in the filter. These options will be explored in future work.

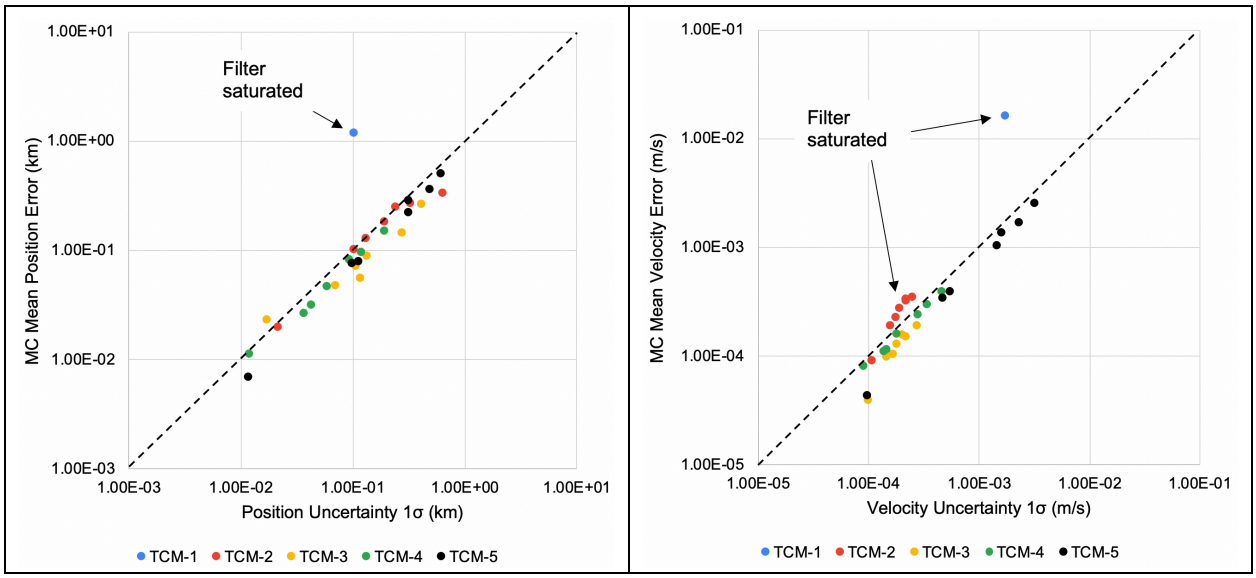

Figure 22. Summary of Monte Carlo analyses with various tracking schedules leading up to each TCM. *Note that there are some cases where the sensitive, nonlinear dynamics lead to filter saturation. These edge cases demonstrate the need for caution during operations.*

These Monte Carlo runs demonstrate multiple trends and events worth discussing in the context of BLT navigation. There are some cases where the covariance estimated by the filter is clearly over-optimistic when compared to the Monte Carlo results. However, for many other cases, the filter covariance is on the same order of magnitude as the Monte Carlo results. These findings demonstrate the need to adjust the filter tuning depending on the dynamical environment – there is not always a single filter tuning that works for all cases.

The navigation requirements analysis resulted in the relationship between navigation accuracy, mission ΔV, and NRHO insertion accuracy. The simulated OD study resulted in the relationship between tracking cadence and navigation accuracy. Given these two relationships, it is now possible to infer the relationship between tracking cadence and mission ΔV and between tracking cadence and NRHO insertion accuracy. It is assumed that there is continuous tracking for the 24 hours between launch and TCM-1, which is common because of the importance of correcting launch vehicle injection errors quickly. For each of the other TCMs, the analyses presented here can be used to prioritize when frequent tracking is most valuable.

VII. Conclusion

The analyses in this paper address a range of questions related to navigating a spacecraft on a BLT to an NRHO. Realistic requirements for launch injection error, tracking cadence, tracking measurement noise, and tracking pass phasing are derived from analysis. Future work will consider additional combinations of the various trades presented here. The sensitivity of the outbound lunar flyby will be studied in order to understand operational requirements for those families of transfers. NASA and Advanced Space will fly a low-energy transfer similar to the ones studied here (without an outbound lunar flyby) with the CAPSTONE mission, currently planned for launch in December 2020.

The authors wish to acknowledge support from the NASA SBIR (Small Business Innovative Research) program, Caltech for the use of Monte software, and Johnson Space Center for the use of Copernicus software.

References

1. Williams J, Lee DE, Whitley RJ, Bokelmann KA, Davis DC, Berry CF. Targeting cislunar near rectilinear halo orbits for human space exploration. *Adv Astronaut Sci*. 2017;160:3125-3144.
2. Parker JS, Anderson RL. *Low-Energy Lunar Trajectory Design*. Hoboken, NJ: John Wiley and Sons; 2014.
3. Parker JS, Bezrouk C, Davis KE. Low-Energy Transfers to Distant Retrograde Orbits. In: *Advances in the Astronautical Sciences Spaceflight Mechanics 2015*. Williamsburg, VA; 2015:AAS 15-311.
4. Koon WS, Lo MW, Marsden JE, Ross SD. Low energy transfer to the moon. 2001:63-73.
5. Chung MKJ, Hatch SJ, Kangas JA, Long SM, Roncoli RB, Sweetser TH. Trans-lunar cruise trajectory design of GRAIL (Gravity Recovery and Interior Laboratory) mission. In: *AIAA/AAS Astrodynamics Specialist Conference 2010*. ; 2010. doi:10.2514/6.2010-8384
6. Parrish NL, Kayser E, Udupa S, Parker JS, Cheetham BW, Davis DC. Survey of Ballistic Lunar Transfers to Near Rectilinear Halo Orbit. *AAS Astrodyn Spec Conf*. 2019:1-20.
7. Parker JS. Families of low-energy lunar halo transfers. *Adv Astronaut Sci*. 2006:AAS 06-132.
8. Jah M, Hughes S, Wilkins M, Kelecy T. The general mission analysis tool (GMAT): A new resource for supporting debris orbit determination, tracking and analysis. In: *European Space Agency, (Special Publication) ESA SP*. ; 2009.
9. Jonathon Smith W. MONTE Python for Deep Space Navigation. *Proc 15th Python Sci Conf*. 2016;(Scipy):62-68. doi:10.25080/majora-629e541a-009
10. Ocampo CA. An Architecture for a Generalized Trajectory Design and Optimization System. In: *International Conference on Libration Points and Missions*. ; 2002.
11. Folkner WM, Williams JG, Boggs DH, Park RS, Kuchynka P. *The Planetary and Lunar Ephemerides DE430 and DE431*. Vol 196.; 2014.
12. Gamper E, Kebschull C, Stoll E. Statistical Orbit Determination using the Ensemble Kalman Filter. *Acta Astronaut*. 2018;(January):22-24.
13. Leonard JM, Cheetham BW, Born GH. Preliminary Evaluation of Earth-Moon Libration Point Orbit Navigation with Post-Processed ARTEMIS Data. In: *24th International Symposium on Space Flight Dynamics*. Laurel, MD; 2014.
14. Parker JS. Establishing a network of lunar landers via low-energy transfers. In: *Advances in the Astronautical Sciences*. ; 2014.
15. Gates CR. *A Simplified Model of Midcourse Maneuver Execution Errors*. Pasadena, CA
16. Oberth H. *Ways to Spaceflight*. R. Oldenbourg Publishing House; 1929.
17. Parrish NL, Bolliger M, Kayser E, et al. Near Rectilinear Halo Orbit Determination with Simulated DSN Observations. In: *Space Flight Mechanics Meeting*. Orlando, FL; 2020.